SLAC-PUB-2508
May 1980
(M)

DIRECT FRAGMENTATION AND HARD-SCATTERING PROCESSES IN RELATIVISTIC HEAVY-ION REACTIONS*

Cheuk-Yin Wong
Oak Ridge National Laboratory
Oak Ridge, Tennessee 37830

and

R. Blankenbecler
Stanford Linear Accelerator Center
Stanford University, Stanford, California 94305

Submitted to Physical Review C

* Work supported in part by the Department of Energy under contract DE-AC03-76SF00515, and by the Division of Basic Energy Science, under the Department of Energy, contract W-7405-ENG-26 with the Union Carbide Corporation.

ABSTRACT

In a relativistic heavy-ion reaction, there are many processes which contribute to fragmentation phenomenon. Here we examine two: the direct fragmentation process in which the detected proton is emitted from a parent nucleus without additional scattering, and the hard scattering process in which a nucleon from one nucleus makes a collision with a nucleon from the other nucleus. In terms of a combination of these two processes, the proton inclusive data of Anderson et al., for the reaction $\alpha + {}^{12}C \rightarrow p + X$ at different bombarding energies can be successfully analyzed. We find that the direct fragmentation process dominates the cross section at 0^{o} and 180^{o}. On the other hand, the hard scattering process dominates the cross section at the quasi-elastic peak when the transverse momentum far exceeds 0.1 GeV/c. Our model leads naturally to a new scaling variable which is the generalization of the Feynman scaling variable for situations when the rest masses are not negligible. As the nuclear momentum distribution enters into the model in a very important way, our analysis constitutes in essence a semi-empirical determination of the nuclear momentum distribution. Furthermore, since a single nucleon can carry a large fraction of the momentum of the parent nucleus in a cooperative manner, relativistic heavy-ion reaction may be utilized to provide valuable information on the high momentum tail of the nuclear momentum distribution when the effects of final state interactions are better understood.

I. INTRODUCTION

Recent experiments using very energetic heavy ion beams have created considerable theoretical interest.[1] Along with several other models, a simple relativistic hard-scattering (RHS) model was put forth for this type of reaction,[2] based on the constituent interchange model originally proposed for high energy hadron scattering.[3] In this model, the constituent structure of the scattering systems and the forces due to the interchange of the constituents are taken into account. The theory can be applied to meson production as well as to the yields of light nuclei. Counting rules involving the Feynman scaling variable x_F were derived to characterize the behavior of the reaction cross section in terms of the short range behavior of the nucleon-nucleon force. This remarkably simple model was found to work quite well in explaining certain experimental data. A similar model using a different kinematic representation[4] was also proposed and found to be useful in analyzing the meson and proton production cross sections in heavy-ion reactions.

In deriving the counting rules for heavy-ion reactions, one considered[2] the case in which the energies of the colliding systems are so large that the rest masses of the nuclei can be neglected. Great simplification of the structure function, the basic reaction cross section and the six-dimensional hard-scattering integral then follows. Counting rules are obtained as the index function of the power of $(1 - x_F)$. While these counting rules are useful results for very energetic heavy-ion collisions, their application directly to heavy-ion collisions at an energy of only 1 to 2 GeV per nucleon may be subject to question. It is perhaps not surprising that after the initial success

of these counting rules for forward pion production some discrepancies for backward pion production[5,6,7] were then found. In the face of such discrepancies, it is important to analyze carefully any error arising from the use of asymptotic functional behavior so as to separate out true physical effects such as constituent clustering[6] and shadowing from simple errors of kinematics. For this reason, one may wish to study the RHS model using exact relativistic kinematics and direct Monte-Carlo integration of the six-fold integral. Indeed,when this was carried out for the pion production case,[8] the experimental $p + {}^{12}C \to \pi^{\pm} + X$ data of Baldin et al.,[9] at the backward angle of 180° can be explained well by the RHS model. Furthermore, the results of a direct numerical integration indicate that the RHS cross section as a function of the Feynman scaling variable behaves differently for the forward and the backward directions. For pion production at $\theta = 0^{\circ}$, the RHS cross section is insensitive to the bombarding energy and scales well with respect to x_F. It obeys approximately the counting rule of Schmidt and Blankenbecler.[2] However, for $\theta = 180^{\circ}$, the kinematics is such that the RHS cross sections obtained from the six-fold RHS integral depend on the energy of the projectile and do not scale well with respect to the Feynman scaling variable x_F. In view of these results, the discrepancies between the data and the counting rules arise simply from using an asymptotic result in a kinematic situation where the conditions for asymptotic behavior are not met. The success of simple scaling for the forward angles may be due to a kinematic effect as was discussed previously.[6]

We undertake to examine another application of the relativistic hard scattering model for the analysis of the proton inclusive data[10]

in the collision of $\alpha + {}^{12}C$. Previously, these data were analyzed by Chemtob[8] using the RHS model. It was concluded that the RHS model could not explain the experimental data. In particular, the decrease in the theoretical cross section in the transverse direction was far too slow. One knows, however, that in the discussion of proton production the hard scattering process is not the only one present. Since the proton is already a constituent of the projectile and the target, there is a very important peripheral process in which the detected proton is fragmented from the parent nucleus without suffering further scattering while the complimentary remnant of the parent nucleus interact with the other nucleus [Fig. 1(a)]. This process, which we call the direct fragmentation process, is in fact the dominating process for the very forward and the very backward angles. One expects therefore from the width of the longitudinal momentum distribution[1] that the direct fragmentation peak also has a transverse momentum width of about 0.1 GeV/c, roughly characteristic of the nuclear size. To analyze the experimental data at 0°, 180° and $p_T > 0.1$ GeV/c, it is necessary to consider a combination of both processes. We shall see later that when both the direct fragmentation and the hard scattering processes are taken into account, theoretical results agree well with the experimental data of Anderson et al.,[10] for the reaction $\alpha + {}^{12}C \rightarrow p + X$.

Another related objective of the present investigation is to study the scaling phenomena in proton production. Our understanding of the scaling phenomena here may shed some light on the analysis of scaling phenomena in other reactions such as in pion production and may supplement other studies of different parametrizations of the cross section.[11]

We shall see later that our model leads naturally to a new scaling variable which is in essence a generalization of the Feynman scaling variable to an energy region where the rest masses of the interacting systems are not small compared to the colliding energies. Along with the success of finding a new scaling variable for proton production, a corresponding scaling variable for pion production has also been uncovered.[12]

In the present analysis (as well as elsewhere in nuclear physics) a very important quantity is the momentum distribution or the related structure function of a nucleon in a nucleus. Although the nuclear momentum distribution is a basic nuclear property which is important in understanding the correlation between nucleons and the behavior of many intermediate energy phenomena involving large momentum transfers,[2,13,14] not much is known experimentally about the general features of this momentum distribution. In the relativistic direct fragmentation process, since the detected proton is emitted by one of the colliding nuclei without additional collision with the other nucleus, it carries much information about the nuclear momentum distribution. Additional final state interactions may distort this distribution but the momentum distribution obtained thereby still provides valuable information which may not be obtained by other means. For example, because the detected proton can carry a large fraction of the momentum of the parent nucleus, it may provide information on the high momentum tail of the nuclear momentum distribution. Indeed, as was emphasized not the least by Anderson et al.,[10] and Schmidt and Blankenbecler,[2] relativistic heavy-ion reaction may prove to be a

useful tool for the extraction of some basic nuclear parameters which are still unknown.

This paper is organized as follows. In Section II, we review the hard scattering model and pave the way for the introduction of the direct fragmentation process in Section III. An intrinsic scaling variable is then introduced and utilized to correlate different sets of experimental data. In Section IV, we study the form of the structure function and parametrize it as a sum of a single-particle part and a correlated part. Detail analysis of the proton inclusive data of Anderson et al., for the $\alpha + {}^{12}C \to p + X$ reaction at various energies and transverse momenta was carried out in Section V. The nuclear momentum distribution obtained thereby is compared with the theoretical results of Zabolitzky and Ey[13] in Section VI. Section VII concludes the present discussion.

II. RELATIVISTIC HARD-SCATTERING (RHS) MODEL

We shall briefly sumarize the main results of the relativistic hard scattering model, both to introduce the notation and also to pave a way for subsequent discussions of the direct fragmentation process. We consider a target nucleus A with a mass m_A and a projectile nucleus B (B stands for Beam) with a mass m_B. Using the infinite momentum frame, we write the target four-momenta A and the projectile four-momenta B as:[2,15]

$$A = \left(P_1 + \frac{A^2}{4P_1} , \vec{0} , -P_1 + \frac{A^2}{4P_1} \right) , \tag{2.1}$$

$$B = \left(P_2 + \frac{B^2}{4P_2} , \vec{0} , P_2 - \frac{B^2}{4P_2} \right) , \tag{2.2}$$

where the letter labels also denote the corresponding momentum four-vectors and the quantities P_1 and P_2 depend on the frame of reference. In particular, in the center of mass frame, we have

$$P_1 = \left[s + A^2 - B^2 + \lambda\left(s,A^2,B^2\right)\right] \Big/ 4\sqrt{s} \quad , \tag{2.3}$$

and

$$P_2 = \left[s + B^2 - A^2 + \lambda\left(s,A^2,B^2\right)\right] \Big/ 4\sqrt{s} \quad , \tag{2.4}$$

where

$$s = (A + B)^2 \quad , \tag{2.5}$$

$$A^2 = m_A^2 \quad , \tag{2.6}$$

$$B^2 = m_B^2 \quad , \tag{2.7}$$

and

$$\lambda^2\left(x_1,x_2,x_3\right) = x_1^2 + x_2^2 + x_3^2 - 2\left(x_1x_2 + x_2x_3 + x_3x_1\right) \tag{2.8}$$

The hard-scattering contribution to the inclusive process $A + B \to C + X$ is represented by the diagram in Fig. 1(b). The nuclei A and B interact through the emission of a virtual subsystem a from A and a subsystem b from B. The subsystems are the ones to scatter through the basic process $a + b \to C + d$ where C is the detected particle. They have off-shell momenta given by:

$$a = \left(xP_1 + \frac{k^2 + k_T^2}{4xP_1} \, , \, \vec{k}_T \, , \, -xP_1 + \frac{k^2 + k_T^2}{4xP_1}\right) \quad , \tag{2.9}$$

$$b = \left(yP_2 + \frac{\ell^2 + \ell_T^2}{4yP_2} \, , \, \vec{\ell}_T \, , \, yP_2 - \frac{\ell^2 + \ell_T^2}{4yP_2}\right) \tag{2.10}$$

where

$$k^2 = \left[x(1-x)A^2 - x\alpha^2 - k_T^2\right] \Big/ (1-x) \quad , \tag{2.11}$$

$$\ell^2 = \left[y(1-y)B^2 - y\beta^2 - \ell_T^2\right]\Big/(1-y) \quad , \tag{2.12}$$

and α^2 (or β^2) is the square of the invariant on-shell mass complementary to a (or b) in nucleus A (or B). If nuclear binding energies are neglected, they become simply

$$\alpha^2 = \left(m_A - m_a\right)^2 \quad , \tag{2.13}$$

and

$$\beta^2 = \left(m_B - m_b\right)^2 \quad , \tag{2.14}$$

where m_a and m_b are the rest masses of a and b respectively. With this parametrization of the off-shell momenta, we get the "momentum fraction x" of the subsystem a in the nucleus A given from Eq. (2.9) by

$$x = \frac{a_0 + a_z}{A_0 + A_z} \quad , \tag{2.15}$$

and the momentum fraction y of the subsystem b in the nucleus B as follows

$$y = \frac{b_0 - b_z}{B_0 - B_z} \quad . \tag{2.16}$$

The relativistic hard scattering (RHS) contribution to the inclusive process A + B → C + X represented in Fig. 1(b) can be shown to lead to an invariant cross section given by

$$E_C \frac{d^3\sigma}{dC^3}\bigg|_{RHS} = \sum_{a,b} \int dx d^2k_T dy d^2\ell_T G_{a/A}(x,\vec{k}_T) G_{b/B}(y,\vec{\ell}_T) r(s',s,x,y) \times E_C \frac{d^3\sigma}{dC^3}(ab \to Cd; s't'u') \quad . \tag{2.17}$$

Here, $r = \lambda(s',k^2,\ell^2)/xy\,\lambda(s,A^2,B^2)$ with $s' = (a+b)^2$. The structure function $G_{a/A}(x,\vec{k}_T)$ is the probability of finding a constituent of type

a in nucleus A with fractional momentum x and transverse momentum $\vec{k}_T$. It is defined in terms of the Bethe-Salpeter bound state wave function $\psi(\vec{p}_a)$ with one leg (α) on-shell by

$$G_{a/A}(x,\vec{k}_T) = \frac{1}{2(2\pi)^3} \frac{x}{1-x} \left|\psi(\vec{p}_A)\right|^2 \quad . \tag{2.18}$$

The quantity $E_C d^3\sigma/d\ c^3(ab \to Cd; s't'u')$ is the invariant cross section for the basic process a + b → C + d written in terms of the basic Mandelstam variables s', t', and u'. The above result, which has simple probabilistic interpretation, was derived by using the Feynman rules and by integrating over the final state phase space.[3]

To carry out the integration of Eq. (2.17), one selects the dominant channel of subsystems a and b, which in the case of pion and proton productions are the nucleons. The six-dimensional integral can be performed with properly parametrized structure functions and the knowledge of experimental basic cross section, the only complication being the relativistic kinematics. We summarize the necessary procedures in Appendix I for the evaluation of the RHS integral.

III. DIRECT FRAGMENTATION PROCESS

In a relativistic heavy-ion reaction, there are many different processes which contribute to "fragmentation" phenomenon, the experimental characteristics of which are quite well known. One such process is the hard scattering process represented by Fig. 1(b) and discussed in the last section. We can envisage another peripheral process in which a subsystem C (proton, in this case) comes out of the nucleus without additional scattering while its complementary remnants

interact with the other nucleus. This process, which we call the direct fragmentation process;[16] is represented by the diagram in Fig. 1(a). Since the proton does not suffer additional scattering, they are likely to emerge near 0^{o} and 180^{o}. All the evidence[1] points to the fact that direct fragmentation dominates the cross section at the very forward and backward angles with a characteristic momentum width of about 0.1 GeV/c. When the transverse mementum of the proton increase much beyond this value, the importance of the direct fragmentation is expected to decrease and other processes will become important. In any case, to understand the proton inclusive data for small values of p_T and to determine the relative importance of the processes, we need a quantitative investigation of the direct fragmentation process.

Following the same steps as in deriving the RHS integral,[3] we can write down (see Appendix II) the direct fragmentation (DF) cross section represented by Fig. 1(b) as follows:

$$E_C \frac{d^3\sigma}{dC^3}\bigg|_{DF} \sim x_D \bar{G}_{C/B}\left(x_D, \vec{C}_T\right) \sum_i \int \frac{d^3 i}{E_i} E_i \frac{d^3\sigma}{di^3} (\beta + A \to i + X') \quad . \qquad (3.1)$$

Here, instead of the momentum variables C_z, we used the momentum fraction x_D introduced in the last section. For projectile fragmentation, x_D is the momentum fraction of the particle C out of the parent nucleus B (of the beam). It is related to C_z by

$$x_D = \frac{C_0 + C_z}{B_0 + B_z} \qquad (3.2)$$

The momentum fraction x_D is a longitudinally invariant quantity. It does not depend on the coordinate frame of reference. The structure function $\bar{G}_{C/B}(x_D, \vec{C}_T)$ is the probability of finding a constituent of type

C in the nucleus B with fractional momentum x_D and transverse momentum $\vec{C}_T$. It is defined in terms of the Bethe-Salpeter bound state wave function with the leg C on shell. The bar symbol on top of $\bar{G}_{C/B}$ indicates that they are in principle different from the structure function $G_{C/B}$ given in Eq. (2.18): the latter quantity being calculated with particle C off shell. The basic invariant cross section $E_i d^3\sigma/di^3$ is for the reaction $\beta + A \to i + X'$. As the measurement of C is inclusive, it is necessary to sum over all distinct channels i and for each channel integrate over all the phase space.

With B representing the beam particles, the expressions in Eq. (3.1) and (3.2) are the direct fragmentation cross section for the projectile direct fragmentation process. We can write down a similar expression for the target fragmentation process:

$$E_C \frac{d^3\sigma}{dC^3}\bigg|_{DF} \sim x_D \bar{G}_{C/A}\left(x_D, \vec{C}_T\right) \sum_i \int \frac{d^3 i}{E_i} E_i \frac{d^3\sigma}{d^3 i}\,(\alpha + B \to i + X') \quad , \tag{3.3}$$

where the momentum fraction x_D is given by

$$x_D = \frac{C_0 - C_z}{A_0 - A_z} \quad . \tag{3.4}$$

The differences in the signs in Eqs. (3.2) and (3.4) arise from the differences in the definition of x and y [see Eqs. (2.15) and (2.16)].

Since projectile fragmentation is mainly associated with $C_z, B_z > 0$ and target fragmentation with $C_z, A_z > 0$, we can often use a common definition for events in this restricted kinematic regime:

$$x_D = \frac{C_0 + |C_z|}{N_0 + |N_z|} \tag{3.5}$$

where N stands for the parent nucleus out of which the particle C is extracted. The less likely events, with $C_z < 0$ when $B_z > 0$ for projectile fragmentation and $C_z > 0$ when $A_z < 0$ for target fragmentation, require the more general definitions of Eqs. (3.2) and (3.4).

One expects that the sum of all the total cross section for all possible channels $\sum_i \int (d^3i/E_i)E_i(d^3\sigma/di^3)(\beta A \to iX')$ depends mostly on the geometrical dimensions of the colliding systems and is therefore rather insensitive to the collision conditions when the collision energy is high enough (above 1 or 2 GeV per nucleon). When this happens, it is reasonable to approximate it by a constant to obtain the result:

$$E_C \frac{d^3\sigma}{di^3}\bigg|_{DF} \sim \begin{cases} x_S \bar{G}_{C/B}(x_D, \vec{C}_T) & \text{projectile fragmentation} \quad (3.6) \\ x_D \bar{G}_{C/A}(x_D, \vec{C}_T) & \text{target fragmentation} \quad (3.7) \end{cases}$$

In this case, in terms of x_D, the cross section should be a universal function, depending only very weakly on s. Thus, when the direct fragmentation process is the dominant process, the fractional momentum x_D can serve as a scaling variable. The subscript D is introduced to denote this direct fragmentation scaling variable, to differentiate it from the Feynman scaling variable x_F given by[17]

$$x_F = \frac{C_z}{C_{max}} \quad , \qquad (3.8)$$

evaluated in the center-of-mass system.

How good a scaling variable is x_D? We can plot the experimental invariant cross section as a function of x_D for various values of $p_T(\equiv C_T)$. We show in Fig. 2 the data of Anderson et al., for $\alpha + {}^{12}C \to p + X$. For each value of the transverse momentum of the

proton p_T, the data points appear to fit in the same curve for different bombarding momentum p_α There are however some deviations for large values of x_D for the data points of $p_\alpha = 0.93$ GeV/c which may be too small for scaling. Data points at higher energies do not seem to suffer this defect. We note also that the data points for small values of $x_D (x_D \gtrsim 0.2)$ at $p_T = 0$ depend on projectile momentum. This region of the proton spectrum contains important contributions from the hard scattering process and from multiple scattering. It should not be given much weight in assessing the direct fragmentation process. Figure 2 indicates that scaling with respect to the intrinsic scaling variable x_D occurs for $\alpha + {}^{12}C \to p + X$ at $x_D \gtrsim 0.2$ and $p_\alpha \gtrsim 1.74$ GeV/c/N.

We note in passing that although we were led to the introduction of x_D as a scaling variable by considering the direct fragmentation process, the results in Figures 2, 3 and 5 below indicate that x_D scaling persists even for $p_T = 0.3$ GeV/c for which the hard scattering process becomes important. We can now understand this phenomena as due to the fact that x_D is also approximately equal to the proper scaling variable for the hard scattering process.[12] Thus, scaling with respect to x_D persists even though there has been a change of the underlying mechanism.

The scaling variable x_D provides a natural way to link the forward projectile fragmentation data with the target fragmentation data pertinent to the same nucleus. For example, we can consider the reaction α (projectile) + ${}^{12}C$ (target) $\to$ p + X. The target fragmentation proton spectrum provides information about $\overline{G}_{p/{}^{12}C}(x_D, C_T)$. Next we consider the inverse reaction ${}^{12}C$ (projectile) + α (target) $\to$ p + X. The projectile fragmentation proton spectrum provides information about

the same structure function $\bar{G}_{p/^{12}C}(x_D, \vec{C}_T)$ but at a different region of x_D. The structure function extracted from forward and backward direction in the two reactions should join on smoothly with respect to each other, Indeed, using the data of $^{12}C + {}^{12}C \to p + X$ to approximate the reaction ^{12}C (projectile) + α (target) $\to$ p + X (allowing for $A_{Target}^{1/3}$ dependence), it appears possible to link the forward data of Papp et al.,[19] with the 180° data of Geaga et al.[18] One notes furthermore that the 180° data of Geaga et al., pertains more to the structure function at large values of x_D and hence is very valuable in extracting information on the high momentum tail of the momentum distribution.

The scaling variable as defined by Eqs. (3.2),(3.4) or (3.5) is just the generalization of the Feynman scaling variable for situations where the rest masses of the colliding systems are not negligible. Consider for example the projectile fragmentation case. In the very high energy limit, we have

$$x_D \sim \frac{2C_z}{2B_z} \sim \frac{C_z}{C_{max}} = x_F \quad , \tag{3.9}$$

since B_z and C_{max} both approach $\sqrt{s}/2$. Thus x_D approaches x_F in the very high energy limit. In the other extreme, for the non-relativistic case,

$$x_D \sim \frac{m_C(1 + v_C/c)}{m_B(1 + v_B/c)} \sim \frac{m_C}{m_B}\left(1 + \frac{v_C - v_B}{c}\right) \tag{3.10}$$

We have

$$x_D - x_0 \cong \frac{m_C}{m_B}\left(\frac{v_C - v_B}{c}\right) \quad , \tag{3.11}$$

where

$$x_0 = \frac{m_C}{m_B} \quad . \tag{3.12}$$

Hence, $x_D - x_0$ is just the velocity difference (from the beam velocity). It is a measure of the intrinsic velocity when the nucleus is at rest and is therefore a good scaling variable for fragmentation.

IV. PARAMETRIZATION OF THE STRUCTURE FUNCTION

We shall consider first the structure function $G_{a/A}(x,k_T)$ and examine the limiting case of x approaching unity for which simple vertex functions have been written down.[2] For a renormalizable interaction between the constitutents, including vector exchange, the falloff of the vertex function arises solely from the constituent propagators. One finds[2]

$$|\psi|^2 \sim \left(k^2 - a_1^2 \right)^{-2T\left(N_A - N_a\right) + 1} \quad , \tag{4.1}$$

where a_1 is a function of the masses of the exchanged mesons and constitutent form factors and is chosen to be a constant for simplicity. The quantity T depends on the interaction[2] and is about three. The members N_A and N_a are the nucleon numbers of nucleus A and a, respectively. From Eqs. (4.1) and (2.18), the structure function can be written in the form

$$G_{a/A}(x,\vec{k}_T) = \frac{x}{1-x} \frac{1}{\left[1 + \dfrac{\bar{k}^2 - k^2}{\left(Dm_A\right)^2}\right]^{g+1}} \quad , \tag{4.2}$$

where the counting index appearing in the counting rules is given by

$$g = 2T\left(N_A - N_a\right) - 1 \tag{4.3}$$

and

$$D^2 = \left(a_1^2 - \bar{k}^2\right)/m_A^2 \quad . \tag{4.4}$$

In Eq. (4.2), k^2 is a function of x and k_T as given by Eq. (2.11):

$$k^2 = \left[x(1-x)m_A^2 - xm_\alpha^2 - k_T^2\right] \Big/ (1-x) \tag{2.11}$$

which has an extremum at

$$x_0 = m_a / m_A \tag{4.5}$$

and

$$k_T = 0 \quad .$$

The quantity $\bar{k}^2$ in Eq. (4.2) is the value of k^2 at the extremum. It is given by the constant

$$\bar{k}^2 = m_A^2 \left(1 - m_\alpha / m_A\right)^2 \simeq m_a^2 \quad . \tag{4.7}$$

Around the extremum, we can expand k^2 in the form

$$k^2 = \bar{k}^2 - \left(m_A / m_\alpha\right)\left[m_A^2 (x - x_0)^2 + k_T^2\right] \tag{4.8}$$

Therefore, the square-bracketed factor in the denominator of Eq. (4.2) near the extremum is given by

$$\left[1 + \frac{\bar{k}^2 - k^2}{(Dm_A)^2}\right]^{g+1} = \left[1 + \left(\frac{m_A}{m_\alpha}\right) \frac{(x - x_0)^2 + k_T^2 / m_A^2}{D^2}\right]^{g+1} \quad . \tag{4.9}$$

As m_A / m_α is not far from unity, the parameter D is a good measure of the width of the fall-off, in units of x and in the direction of x and k_T.

Near the region of $x \sim 1$, the denominator in Eq. (4.2) controls the behavior of G and we have

$$\lim_{x \to 1} G\left(x, \vec{k}_T\right) \sim (1-x)^g \quad , \tag{4.10}$$

while its large k_T behavior is

$$\lim_{k_T \to \infty} G\left(x, \vec{k}_T\right) \sim \left(k_T^2\right)^{-g-1} \quad . \tag{4.11}$$

These are the desired properties of the structure function as discussed previously.[2]

Since the experimental data cover a large region of x values, we are interested in the structure function not only in the region of large momentum $x \sim 1$ but also in the region of zero intrinsic momentum x_0. In order to avoid the introduction of additional parameters[2,8] so that the structure function peaks at the desired location of x_0, we find it more convenient to work with the form (4.2) instead of extracting a factor of $(1-x)^g$ explicitly as was done previously.[2,8] We note that the extremum of the probability distribution $|\psi|^2 \left(=(1-x)G(x,k_T)/x\right)$ is located at the same point as the extremum of k^2; that is, at $x_0 = m_a/m_A$ and $k_T = 0$.

The structure function given in Eq. (4.2) with a relatively large width parameter D (of the order of 0.5) is the structure function for the high-momentum tail. It corresponds to the component of the structure function resulting from the correlation of <u>all</u> of the constituent nucleons. The large value of D also implies a large mass parameter or equivalently a small correlation length. Although the structure function so obtained shows a peak at the point $x \sim x_0$, it cannot represent well the structure function near that region of small intrinsic momentum. We know as a matter of fact that near the region of small intrinsic momentum the nucleon motion is governed by independent particle model where the nucleons are completely uncorrelated and the length parameter

is about the size of the nucleus. There is an additional component of the structure function which arises from the single-particle motion of nucleons. We can parametrize this component with a different index p and a small width parameter δ where $\delta << D$. The total structure function is then the sum of these two components which we write in the form

$$G_{a/A}(x,\vec{k}_T) = \frac{x}{1-x}\left[\frac{g_1}{\left\{1+\frac{\bar{k}^2-k^2}{(\delta m_A)^2}\right\}^p}+\frac{g_2}{\left\{1+\frac{\bar{k}^2-k^2}{(Dm_A)^2}\right\}^p}\right]\frac{1}{\left\{1+\frac{\bar{k}^2-k^2}{(Dm_A)^2}\right\}^{g-p+1}} \tag{4.12}$$

where the first term inside the square bracket represents the single-particle contribution while the second term the multiparticle correlation. Since there is a range of values of p and δ which fits the data, we choose p to have the value six (corresponding to the counting index for the constituent in a two-body system). The parameters g_1, g_2, δ and D are then determined by comparing with experiment. Of course, more complicated wave functions based on the above type of reasoning can be written down and more accurate data may require their use.

The above discussion deals with the structure function $G_{a/A}(x,\vec{C}_T)$ which appears in the six-fold relativistic hard-scattering integral. The structure function $\overline{G}_{a/A}(x,\vec{C}_T)$ which enters in the direct fragmentation process is in principle different from $G_{a/A}(x,\vec{C}_T)$. We have chosen to define $\overline{G}_{a/A}(x,\vec{C}_T)$ (see Appendix II) in such a way that $\overline{G}_{a/A}$ and $G_{a/A}$ differ only by the vertex function ϕ. In fact, the vertex function $\bar{\phi}_a(\vec{p}_A)$ for $\overline{G}_{a/A}(x,\vec{C}_T)$ and $\phi_A(\vec{p}_A)$ have the same structure but differ only in the on-shell or off-shell properties of the external connecting lines. To the extent that it does not matter which external line is off-shell (this is rigorously correct in the nonrelativistic limit), the vertex

functions ϕ and $\bar{\phi}$ can be set (approximately) equal. Hence the structure function G and $\bar{G}$ can be taken to be the same.

V. ANALYSIS OF THE $\alpha + {}^{12}C \to p + X$ data

Combining both the direct fragmentation and the hard scattering contributions, we can write down the total invariant cross section for the inclusive $A + B \to C + X$ process as

$$E_C \frac{d^3\sigma}{dC^3} = x_D G_{C/N}(x_D, \vec{C}_T) + wE_C \left.\frac{d^3\sigma}{dC^3}\right|_{RHS} , \qquad (5.1)$$

where the subscript N in the structure function stands for the beam nucleus B in the case of projectile fragmentation and nucleus A in the case of target fragmentation. The quantity $E_c d^3\sigma/d^3C\big|_{RHS}$ is the relativistic hard scattering cross section given by Eq. (2.17). As our theory cannot (yet) predict absolute cross sections, the constant w is introduced to adjust the relative importance of the two different processes. It will be determined by comparing with experimental data at different p_T values.

To apply the present model to a concrete example, we focus our attention on the projectile fragmentation data of Anderson et al.,[12] for the reaction $\alpha + {}^{12}C \to p + X$. Since the direct fragmentation term dominates for $p_T \sim 0$, one can attempt to fit the data at $p_T = 0$ with just the first term and obtain an approximate structure function. Final adjustments of the parameters are then made by comparing the experimental data and Eq. (5.1) after evaluating the relativistic hard-scattering integral of Eq. (2.17). We find the following final best set of

parameters for the structure function $G_{p/\alpha}(x,\vec{C}_T)$:

$$\left.\begin{aligned} g_1 &= 0.288\times 10^6 \quad \left(\text{mb } c^3/\text{sr } (\text{GeV})^2\right) \\ g_2 &= 0.234\times 10^4 \quad \left(\text{mb } c^3/\text{sr } (\text{GeV})^2\right) \\ D &= 0.38 \\ \text{and} \qquad \delta &= 0.062 \quad . \end{aligned}\right\} \tag{5.2}$$

Here, to make the analysis of the experimental data simple, we shall not attempt to normalize the structure function but shall let it be calibrated with the experimental cross sections so that the structure function gives directly the invariant cross section. Hence, the coefficients g_1 and g_2 acquires the units as given above. As G is undetermined up to a constant, future use of our structure function should take into account other possible ways of normalizing.

We note in passing that the tail of the structure function $G_{p/\alpha}(x_D,p_T)$ at $x_D \sim 0.3$ to 0.4 can be approximated by a function of the form $(1-x_D)^{26}$. The index of 26 is greater than the value of $g = 6\times 4 - 7 = 17$ predicted by the counting rule. This is as it should be, because we are quite far from the asymptotic region of $x_D \sim 1$. Nevertheless, the counting rule index g gives an order of magnitude guide to the falloff power index of the structure function, when the proper variable x_D is used instead of x_F. In this intermediate x region, one achieves very good fits by changing the parameter from the value T = 3 in Ref. 2 to the value $T \simeq 4$.

We need also the structure function of a proton out of the ^{12}C nucleus, in order to evaluate the hard-scattering integral (2.17). For this purpose, we examine the projectile fragmentation data of Papp et al.;[19]

in the reaction $^{12}C + {}^{12}C \to p + X$ and the target fragmentation data of Geaga et al.,[18] in the reaction α (projectile) + ^{12}C (target) $\to p + X$. To make the comparison quantitative, we need to convert the data of $^{12}C + {}^{12}C$ into an approximate set of data for ^{12}C (projectile) + α (target). This conversion can be done by noting that as a function of target mass A_T, proton inclusive cross section for $x \sim x_0$ is approximately proportional[10] to $A^{1/3}$. We therefore multiply the $^{12}C + {}^{12}C$ cross sections of Papp et al., by a factor of $(4/12)^{1/3}$ so that we can treat them as the cross section for the $^{12}C + \alpha$ system. The data of Papp et al., is given for a laboratory angle of 2.5°, while the data of Geaga et al.,[15] is given for a laboratory angle of 180°. For these angles, the hard-scattering contribution to the cross section is negligibly small compared to the direct fragmentation process. These data can be analyzed using only the first direct fragmentation term in Eq. (5.1). After properly transforming the relevant momentum variables into the scaling variable x_D, taking special care that the transformation for projectile fragmentation is different from target fragmentation (Eqs. (3.2) and (3.5)), we can represent the different sets of experimental data in terms of a single structure function. We find the following set of parameters for the structure function which give a good fit to the 2.5° data of Papp et al.,[19] and the 180° data of Geaga et al.:[18]

$$\left.\begin{aligned} g_1 &= 0.50 \times 10^7 \ \left(\text{mb } c^3/\text{sr } (\text{GeV})^2\right) \\ g_2 &= 0.12 \times 10^5 \ \left(\text{mb } c^3/\text{sr } (\text{GeV})^2\right) \\ D &= 0.30 \\ \delta &= 0.024 \end{aligned}\right\} \qquad (5.3)$$

In this case, the tail of the structure function can be represented by $(1-x_D)^{107}$. This index of 107 is greater than the counting index of $g = 6 \times 12 - 7 = 65$ from the counting rule with $T = 3$, indicating that we are still quite far from the asymptotic region of $x \sim 1$. The value $T = 4 \sim 5$ yields a better value for the index in this region.

Finally, to evaluate the hard-scattering integral, we need the basic cross section for the process $p + p \to p + X$. We note that the elastic cross section can adequately represent this cross section. We therefore parametrize the basic cross section as[20]

$$E_C \frac{d^3\sigma}{dC^3}(pp \to pp) = S\, e^{Bt'}\, \delta\left[(a+b-C)^2 - d^2\right] \qquad (5.4)$$

where B is the slope parameter, S is a constant and t' is the Mandelstam variable in the basic system

$$t' = (b-C)^2 \quad . \qquad (5.5)$$

In terms of the other Mandelstam variable for the basic system

$$s' = (a+b)^2 \quad , \qquad (5.6)$$

we parametrized slope parameter B for pp elastic cross section in the following form

$$\left.\begin{aligned} &(1) \quad B = 0 \ \text{ for } s' \le 4\ (\text{GeV}/c)^2 \quad , \\ &(2) \quad B = 5(s'-4) + 0.36(s-4)^2\ (\text{GeV}/c)^{-2} \\ &\qquad \text{for } 4(\text{GeV}/c)^2 \le s' \le 5.45(\text{GeV}/c)^2 \quad , \\ &\text{and} \quad (3) \quad B = 8(\text{GeV}/c)^{-2} \text{ for } 5.45(\text{GeV}/c)^2 \le s' \ . \end{aligned}\right\} \qquad (5.7)$$

The above parametrization is based on the tabulation of the slope parameter of Benary et al. [20]

The magnitude of the coefficient w which determines the relative importance of the direct fragmentation term and the hard-scattering term is obtained by fitting the experimental data at p_α 1.74 GeV/c for $p_T = 0.3$ GeV/c. There, as the two different terms become dominant at different regions of x_D, the shape of the total contribution depends sensitively on this coefficient. The best value of the product Sw is

$$Sw = 0.318 \times 10^{-11} \left(\text{mb } C^3/\text{sr } (\text{GeV})^2 \right) (\text{MeV/c})^{-4} \quad . \qquad (5.8)$$

Figure 3 gives the comparison of the experimental data with the theoretical results for the reaction α (projectile) + ^{12}C (target) → p + X at a projectile momentum of 1.74 GeV/c per projectile nucleon. This momentum corresponds to a kinetic energy of 1.04 GeV per nucleon. The invariant cross section is plotted as a function of x_D for various values of the transverse momenta of the detected proton p_T. Figure 3(a) shows the results for $p_T = 0$ and Fig. 3(b) for $p_T = 0.3$ GeV/c. As one can see, the data points for $x_D \gtrsim 0.20$ can be well fitted by the theoretical calculations. To study the results in more detail, we can decompose the sum of the theoretical cross sections in terms of the direct fragmentation component and the hard-scattering component. We consider first the case of $p_T = 0$ at $\theta = 0^\circ$. We find that the direct fragmentation dominates for $x_D \gtrsim 0.25$ but the hard-scattering cross section becomes greater than the direct fragmentation cross section for $x_D \lesssim 0.18$. It is worth noting that the tail of the hard-scattering component is similar in shape to that of the structure function represented by the direct fragmentation component, as pointed out previously in Ref. 2. In the region of small x_D, the sum of the direct fragmentation and hard-scattering cross section is still

substantially lower than the experimental cross section, indicating that other processes need to be further included to provide a good fit for this region. We note that the hard-scattering cross section includes a sum over all channels. What we have taken into account so far is only the elastic p,p channel. This is good enough in the region of $x_D \gtrsim 0.20$. However, for the production of lower energy protons, the inelastic channels need to be included. Indeed, it is observed that when the inelastic p,p cross section is taken into account, the hard-scattering cross section for small x_D values is enhanced substantially.[8] It is expected that the hard-scattering process (including both elastic and inelastic pp reactions) dominates over the direct fragmentation process for small values of x_D.

The separation of the forward proton spectrum into a direct fragmentation region ($x_D \gtrsim 0.20$) and a hard scattering region ($x_D \lesssim 0.20$) is consistent with other pieces of experimental data. It is known that the cross section in the region $x_D \gtrsim 0.2$ increases with the target mass as $A_T^{1/3}$, indicating a peripheral nature of the encounter, as would be expected of a direct fragmentation process. On the other hand, the cross section in the region of $x_D \sim 0.10$ increases with the target mass as $A_T^{2/3}$, indicating a geometrically more central nature of the encounter, as would be expected of a hard-scattering process. Also, in a hard-scattering event, since the angular distribution of the basic process becomes more and more isotropic as energy decreases, it is easier for slow protons to come out in the forward direction, even though the constituent particles a and b may not be initially aligned in that direction. Therefore, the hard-scattering cross section for small values

of x_D should increase with decreasing energy. Experimentally, the cross section for $x_D \sim 0.10$ indeed increases when the bombarding energy decreases.

We examine now the forward proton inclusive spectrum for the reaction of $\alpha + {}^{12}C \rightarrow p + X$ at the same projectile momentum (1.74 GeV/c/N) and a transverse momentum of 0.3 GeV/c for the detected proton. Figure 3(b) shows that the experimental data points can be well fitted by the theoretical calculations. We can study the two different components in some detail. One finds that the direct fragmentation dominates when $x_D \gtrsim 0.32$ whereas hard-scattering dominates for $x_D \lesssim 0.28$. It is clear from the shape of the experimental spectra that a combination of the two processes is necessary to explain the experimental data.

We note that in the case of $p_T = 0.3$ GeV/c, the peak of the cross section is given mainly by the hard-scattering process. This is in contrast to the $p_T = 0$ case where the peak of the cross section is given mainly by the direct fragmentation process. Such a change in roles may not be surprising because the direct fragmentation peak has a momentum width σ_p of the order of 0.10 GeV/c.[1] So, at $p_T = 3\ \sigma_p$ the direct fragmentation peak drops down much below the hard-scattering peak. The increasing importance of the hard-scattering component also explains the peculiar phenomenon[10] that the observed momentum width is different in the transverse and in the longitudinal direction. In the transverse direction, the additional contribution and later the dominance of the hard-scattering process give a larger width to the transverse momentum distribution, as compared to the width of the longitudinal momentum distribution at $p_T = 0$.

The interplay between the direct fragmentation and hard-scattering processes can be further displayed by considering the proton transverse momentum distribution for a fixed value of momentum 1.75 GeV/c in the bombardment of ^{12}C with alpha particles at $p_\alpha = 1.74$ GeV/c per nucleon. The experimental data and the theoretical results are shown in Fig. 4. As one observes, the experimental data are quite well reproduced. One can further compare the contributions from the direct fragmentation process and the hard-scattering process. For this momentum, the direct fragmentation process dominates the cross section at $p_T = 0$ whereas the hard-scattering process dominates the cross section at $p_T >> 0.1$ GeV/c. The cross over of the two processes occurs at $p_T \sim 0.2$ GeV/c. It is clear that the direct fragmentation process by itself or the hard-scattering process by itself cannot explain the data. A combination of these two different processes is necessary.

Figure 5 gives the comparison of the experimental data with theoretical results for the reaction of $\alpha + {}^{12}C \rightarrow p + X$ at a momentum of 2.88 GeV/c/N per projectile nucleon. This momentum corresponds to a kinetic energy of 2.09 GeV per nucleon. Figure 5(a) shows the results for $p_T = 0$ and Fig. 5(b) for $p_T = 0.3$ GeV/c. Again, the experimental data points, with the exception of the low momentum region $x_D \lesssim 0.20$, can be well accounted for. The region of small x_D, as we mentioned before, may involve more complex processes and is not expected to be given just by the direct fragmentation process and a hard-scattering process involving only the elastic pp channel. The decomposition of the theoretical cross section into the two underlying components gives features which are the same as in the case of 1.74 GeV/c. They need not be discussed again.

It is worth noting that the theoretical hard-scattering cross section at 2.88 GeV/c is smaller than that at 1.74 GeV/c for small values of x_D. As we explained previously, this is due to the fact that the basic p,p cross section becomes more forward peak as energy increases. So, in order to come out in the forward direction, the colliding constituent nucleons need to align well in the forward direction and hence only a more restricted region of phase space leads to a slow proton in the forward direction as compared to the case of a lower energy collision. This decrease of cross section in this region of small x_D with increasing energy cannot go on without limit. We know that the slope parameter for the basic cross section, which determines the angular anisotropy of the basic reaction, becomes a constant when s' exceeds about 5.5 $(GeV/c)^2$. One therefore expects that as a function of bombarding energy of the heavy ion, the hard-scattering cross section due to the p,p elastic channel in the region of small x_F reaches an approximately constant value when the bombarding energy goes beyond 3 to 4 GeV/nucleon.

Figure 5(b) shows the inclusive proton spectra for $p_\alpha = 2.88$ GeV/c/N and $p_T = 0.3$ GeV/c. As one can see, the theoretical results agree well with experiment for $x_D \gtrsim 0.2$. Again, the region of small values of x_D may have contributions from other processes and has therefore a larger cross section than the calculated results. The peak cross section is due to the hard-scattering process. The cross section at large values of x_D comes mainly from the direct fragmentation process, the hard-scattering process nevertheless gives a substantial contribution to the sum.

In Figure 6, we show the transverse momentum distribution for the case of $p_\alpha = 2.88$ GeV/c/N for a proton momentum of 2.88 GeV/c. The direct fragmentation component again dominates at $p_T = 0$ while the hard-scattering process dominates at $p_T >> 0.1$ GeV/c.

VI. NUCLEAR MOMENTUM DISTRIBUTION

In the model we have presented, the nuclear structure function enters in a very important way. It arises in the direct fragmentation term and also in the hard-scatteing term. The structure function obtained thereby may have already been subject to distortion due to additional final state interactions. It may also need other corrections because of the various approximations introduced to lead to the simplified result of Eq. (5.1). Nevertheless, an analysis of the experimental data in terms of these structure functions is in essence a semiempirical determination of the structure function as defined in the present model. A comparison of the semiempirical and theoretical results will reveal much information about the underlying physics of the structure function and/or final state interactions.

Rather than comparing the structure function, it is more convenient to compare the momentum distribution $P_{a/A}\left(x,\vec{C}_T\right)$ which is related to $G_{a/A}\left(x,\vec{C}_T\right)$ by

$$P_{a/A}\left(x,\vec{C}_T\right) = \frac{x}{1-x}\, G_{a/A}\left(x,\vec{C}_T\right) \quad . \tag{6.1}$$

Recently, momentum distribution for the ground state of ^{4}He has been calculated using various two-body interactions. It was pointed out that a measurement of the momentum distribution, particularly the region at high momentum, will be of great value in understanding the correlation

of nucleons in nuclei. This is in line with the suggestion of Ref. 2 that experimental data of large values of x reveals the degree of many-particle correlations of a composite system. The momentum distribution has been calculated by Zabolitzky and Ey[13] in a non-relativistic coupled-duster form of the many-body theory. To make the comparison possible, we go to the projectile frame in which the center of mass of the projectile is at rest. This is achieved by transforming x_D to $p_z^{(P)}$ in the projectile frame by

$$p_z^{(P)} = m_B \left(x_D - \frac{m_{C\perp}}{m_B} \right) \left(1 + \frac{m_{C\perp}}{m_B x_D} \right) \Big/ 2 \quad , \tag{6.2}$$

where

$$m_{C\perp} = \left(m_C^2 + C_T^2 \right) \quad . \tag{6.3}$$

When the momentum distribution of a nucleon in ^{4}He obtained in the present model is compared directly with theoretical calculations of Zabolitzky et al., one observes that the semiempirical distribution obtained is too narrow compared with the theoretical momentum distribution. The general shape is however similar. In particular, there is a discontinuity in slope at $p_z \sim 1$ ($\hbar$ fm^{-1}) which mimics the change in slope at $p \sim 2$ ($\hbar$ fm^{-1}) in the theoretical calculation. The theoretical calculation demonstrates that the abrupt change in the slope of the momentum distribution originates from the presence of correlations between nucleons. Final state interactions may distort the momentum distribution but are not expected to introduce such abrupt slope changes. Thus, the observed discontinuity in slope may be tentatively taken as a possible evidence for the presence of nuclear correlation of nucleons in the ground state of ^{4}He. More definite conclusions must await further studies of the effects of final state interactions.

VII. CONCLUSIONS AND DISCUSSIONS

With the introduction of the direct fragmentation process to supplement the hard-scattering process, the experimental data of Anderson et al.,[10] can be well explained. We find that direct fragmentation dominates the cross section at $\theta = 0^{\circ}$ and 180° and also the production of very energetic protons for $\theta \neq 0$. On the other hand, the hard-scattering process dominates near the quasi-elastic peak when $p_T >> 0.1$ GeV/c.

Our model leads naturally to a new scaling variable x_D which measures the fractional momentum of the detected fragment relative to the parent nucleus. When plotted in terms of this scaling variable, the invariant cross sections show little energy dependence, except for region of small x_D. Such a scaling behavior can be understood within the context of our present model. In the region where direct fragmentation dominates, only one structure function is necessary to describe the behavior of the cross section at all energies when the energy is high enough. As the structure function depends only on x_D and $\vec{C}_T$, we have scaling in terms of x_D for different values of $\vec{C}_T$. In the quasi-elastic peak when $p_T \neq 0$, the hard-scattering model has a scaling variable which is approximately equal to x_D even for moderate values of p_T.[12]

The analysis of this experimental data provides us with some insight into the momentum distribution of a nucleon in a nucleus. Heavy-ion reactions thus may be a unique tool in probing the high momentum tail of the nuclear momentum distribution. This is possible because a single nucleon can be emitted in a cooperative manner with a large fraction of

the total momentum of the nucleus. Our analysis indicates the possible presence of nuclear correlations in ^{4}He and/or final state interactions. Similar conclusion was also reached by Geaga et al.,[21] from their work in backward proton productions.

Since knowledge of the nuclear momentum distribution can be very useful in nuclear structure and nuclear reaction studies, it is important to develop further both theoretical and also experimental tools for its exploitation. As far as experimental investigations are concerned, what is desirable is a systematic inclusive proton and composite particle production for various nuclei at 0^o and 180^o where only the direct fragmentation is important. The 0^o data give the structure function close to the region of zero intrinsic momentum while the 180^o data give the structure function in the region of large intrinsic momentum. To allow the two structure functions to join on smoothly, one wishes to push the 0^o measurement to as large a momentum as possible and to push the 180^o measurement to as low a momentum as possible. To subtract away the contributions due to the hard-scattering process, it is desirable to have measurements around $P_T \neq 0$ so that the hard-scattering contributions can be well identified. Furthermore, it is desirable to perform experiments at different energies to check whether or not scaling is achieved. Once scaling is achieved, the use of different projectile and target nuclei will aid in determining the counting rules for the dependence of the cross section on the constituent numbers. These scaling laws are the minimal systematics against which new degrees of freedom may appear as peculiar deviations.

Theoretically, much more work remains to be done to examine the corrections to the presence model and the energy dependence of the neglected factor in the direct fragmentation term. Future work should also be directed towards a more careful examination of the structure function and its momentum dependence. It is particularly important to study the effects of final state interactions.[22] By improving both the theoretical and experimental tools we can expect to enlarge our knowledge of some basic and important properties of the nucleus which up to now is still very rudimentary.

ACKNOWLEDGMENT

The authors wish to thank Dr. S. Nagamiya and Dr. G. R. Satchler for helpful discussions and communications. They also wish to thank Dr. J. V. Geaga for sending them the 180^{o} data for $\alpha + {}^{12}C \rightarrow p + X$ before publication.

REFERENCES

1. A good review of recent experimental and theoretical work in this area is found in S. Nagamiya, Proceedings of the Symposium on Heavy Ion Physics from 10 to 200 MeV/AMU, July16-20, 1979, Brookhaven National Laboratory (BNL-51115, 1979). See also A. S. Goldhaber and H. H. Heckman, Annu. Rev. Nucl. Particle Science 28, 161 (1978).

2. E. A. Schmidt and R. Blankenbecler, Phys. Rev. D15, 332 (1977), R. Blankenbecler, Lectures presented at Tubingen University, Tubingen, Germany, June 1977, SLAC-PUB-2077. I. A. Schmidt, SLAC Report No. 203, 1977.

3. For a general review, see D. Sivers, S. J. Brodsky, R. Blankenbecler, Physics Reports 23C, No. 1 (1976).

4. R. L. Hatch and S. E. Koonin, Phys. Lett. 81B, 1 (1978).

5. S. Chessin, J. Geaga, J. E. Grossiord, D. Hendrie, L. Schroeder, B. Treuhaft, K. Van Biber and E. Wuest, Bull. Am. Phys. Soc. 23, 48 (1978).

6. R. H. Landau and M. Gyulassy, Phys. Rev. D19, 149 (1978).

7. L. S. Schroeder, S. A. Chessin, J. V. Geaga, J. Y. Grossiord, J. W. Harris, D. L. Hendrie, R. Treuhaft and K. Van Bibber, Phys. Rev. Lett. 43, 1787 (1979).

8. M. Chemtob, Nucl. Phys. A314, 387 (1979).

9. A. M. Baldin et al., Yad. Fiz. 20, 1201 (1974) (Sov. Jour. Nucl. Phys. 20, 629 (1975)).

10. L. M. Anderson, Jrs. Ph.D. Thesis, University of California at Berkeley, 1977, LBL-6769; L. M. Anderson Jrs., O. Chamberlain, S. Nagamiya, S. Nissen-Meyer, D. Nygren, L. Schroeder, G. Shapiro and H. Steiner, LBL-9493, 1979.

11. S. Frankel, Phys. Rev. Lett. 38, 1338 (1977); G. Berlad, A. Dar and E. Eilam, Phys. Rev. D13, 161 (1976); A. Dar and Tran Thanh Van, Phys. Lett. 65B, 455 (1976).

12. C. Y. Wong and R. Blankenbecler, Proceedings of the Workshop on Nuclear Dynamics, Granlibakken, California (1980), LBL-Report-10688 (1980) and to be published.

13. J. G. Zabolitzky and W. Ey, Phys. Lett. 76B, 527 (1978).

14. R. D. Amado and R. M. Woloshyn, Phys. Rev. C15, 2200 (1977); R. D. Amado, Phys. Rev. C14, 1264 (1976); J. W. Van Orden, W. Truex and M. K. Banerjee, University of Maryland Report (to be published).

15. We have chosen the components A_z, B_z to have the opposite sign of those in Schmidt and Blankenbecler (Ref. 2). The beam B now appears to come from the right and to point in the positive Z direction when Eqs. (2.3) and (2.4) are used.

16. For non-relativistic (d,p) reactions, this process is the well-known Serber stripping process (R. Serber, Phys. Rev. 72, 1008 (1947)). The present analysis is a generalization of the Serber stripping process to heavy-ion reactions using the scaling variable x_D.

17. R. Feynman, Phys. Rev. Lett. 23, 1415 (1969).

18. J. V. Geaga et al., private communication.

19. J. Papp, Ph.D. Thesis, University of California at Berkeley, 1975, LBL-3633; J. Papp, J. Jaros, L. Schroeder, J. Staples, H. Steiner, A. Wagner and J. Wiss, Phys. Rev. Lett. 34, 601 (1975).

20. O. Benary, L. R. Price and G. Alexander, Lawrence Berkeley Laboratory Report UCRL-20000, August 1970.

21. J. V. Geaga et al., (to be published).

22. R. D. Amado and R. M. Woloshyn, Phys. Lett. 69B, 400 (1977).

APPENDIX I

EVALUATION OF THE HARD-SCATTERING INTEGRAL

We present here the detail steps and relativistic kinematics which allows one to evaluate the hard-scattering integral. For a given projectile kinetic energy per nucleon ε we have the invariant scaler variable $s = (A + B)^2$ given by

$$s = A^2 + B^2 + 2m_A\left(N_B\varepsilon + m_B\right) \quad . \tag{I.1}$$

The maximum value of $|\vec{C}|$ can be determined by assuming a minimum missing mass D_{min}

$$C_{max} = \lambda\left(s, C^2, D_{min}\right)\Big/2\sqrt{s} \quad , \tag{I.2}$$

where

$$\lambda^2\left(x_1, x_2, x_3\right) = x_1^2 + x_2^2 + x_3^2 - 2\left(x_1x_2 + x_2x_3 + x_3x_1\right) \quad . \tag{I.3}$$

The knowledge of C_{max} allows one to convert the proton momentum into Feynman's scaling variable and vice versa. In terms of the momentum C_0 and C_Z of the detected proton in the center-of-mass frame, the other invariant variables $t = (B - C)^2$ and $u = (A - C)^2$ are

$$t = -2\left[C_0\left(P_2 + B^2/4P_2\right) - C_Z\left(P_2 - B^2/4P_2\right)\right] + m_B^2 + m_C^2 \quad , \tag{I.4}$$

and

$$u = -2\left[C_0\left(P_1 + A^2/4P_1\right) - C_Z\left(P_1 - A^2/4P_1\right)\right] + m_A^2 + m_C^2 \quad , \tag{I.5}$$

where P_1 and P_2 are given by Eq. (2.3) and (2.4).

Our task is to evaluate the six-dimensional integral for a given set of values of s, t and u. The integration variables are x, y, $\vec{k}_T$ and $\vec{\ell}_T$, but they are restricted in the elastic channel by the delta

function $\delta\left[(a + b + C)^2 - d^2\right]$. We can convert this energy conservation condition into an equation for y:

$$(a + b - C)^2 - d^2 = \left(A_1 y^2 + A_2 y + A_3\right)/(1 - y) = 0 \quad . \tag{I.6}$$

Here the coefficients A_1, A_2 and A_3 are

$$A_1 = -\left[x\bar{s} - 2\left(C_0 - C_Z\right)P_2\right] \quad , \tag{I.7}$$

$$A_2 = -A_1 + m_B^2 - m_\beta^2 - m_B^2\left[m_{a\perp}^2/x\bar{s} - 2\left(C_0 + C_Z\right)/4P_2\right] - X \quad , \tag{I.8}$$

$$A_3 = \left(m_B^2 - m_\beta^2 - \ell_T^2\right)\left[m_{a\perp}^2 - 2\left(C_0 + C_Z\right)/4P_2\right] - \ell_T^2 + X \quad , \tag{I.9}$$

and

$$X = -2\left(C_0 + C_Z\right)P_1 x - 2\left(C_0 + C_Z\right)m_{a\perp}^2/4P_1 x + k^2 + c^2 - m_d^2$$

$$-2\vec{k}_T \cdot \vec{C}_T + 2\vec{\ell}_T \cdot \vec{C}_T + 2\vec{k}_T \cdot \vec{C}_T \quad , \tag{I.10}$$

where

$$\bar{s} = \frac{1}{2}\left[s - A^2 - B^2 + \lambda\left(s, A^2, B^2\right)\right] \quad , \tag{I.11}$$

and

$$m_{a\perp}^2 = k^2 + k_T^2 \quad . \tag{I.12}$$

Therefore, the delta function in the basic cross section becomes

$$\delta\left[(a + b - C)^2 - m_d^2\right] = \frac{1 - y_1}{A_1\left|y_1 - y_2\right|}\,\delta\left(y - y_1\right) + \frac{1 - y_2}{A_1\left|y_1 - y_2\right|}\,\delta\left(y - y_2\right) \quad , \tag{I.13}$$

where y_1 and y_2 are the two solutions of y for Eq. (I.6). An integration over y reduces the six-fold integral into a five-fold integral. In each of the five-dimensional points, there are two contributions from two values of y. Because of the rapid fall-off of the structure function

the point closest to $y_0 = m_b/m_B$ gives the greatest contribution to the integrand.

The knowledge of x, y, $\vec{k}_T$ and $\vec{\ell}_T$ now allow us to evaluate the Mandelstam variables $s' = (a + b)^2$, $t' = (b - C)^2$, $u' = (a - C)^2$ in the basic system. They are given by

$$s' = xy\bar{s} + m_{a\perp}^2 m_{b\perp}^2 / xy\bar{s} - 2\vec{k}_T \cdot \vec{\ell}_T + k^2 + \ell^2 \quad , \tag{I.14}$$

$$t' = -2(C_0 - C_Z)P_2 y - 2(C_0 + C_Z)m_{b\perp}^2/4P_2 y + 2\vec{\ell}_T \cdot \vec{C}_T + \ell^2 + C^2 \quad , \tag{I.15}$$

and

$$u' = -2(C_0 + C_Z)P_1 x - 2(C_0 - C_Z)m_{a\perp}^2/4P_1 x + 2\vec{k}_T \cdot \vec{C}_T + k^2 + C^2 \quad , \tag{I.16}$$

where

$$m_{b\perp}^2 = \ell^2 + \ell_T^2 \quad . \tag{I.17}$$

The function $\lambda(s,s',x,y)$ and $d\sigma/dt'(pp)$ which are given in terms of s' and t', can now be determined. With the structure functions already given in the variables of x, y, $\vec{k}_T$ and $\vec{\ell}_T$, the complete integrand can now be evaluated. The hard scattering integral can be evaluated by a Monte Carlo sampling of the five dimensional integration points in x, $\vec{k}_T$ and $\vec{\ell}_T$, with convenient changes of variables to put more weights to the regions of large contributions.

APPENDIX II

DIRECT FRAGMENTATION CROSS SECTION

Following Ref. 3, we write down the differential cross section for the process $AB \to CiX'$ depicted in Fig. 1(a) as

$$d\sigma(AB\to CiX') = \frac{1}{2E_A 2E_B \left|v_A - v_B\right|} \sum_i \left|M_{AB\to CiX'}\right|^2 dp \quad , \tag{II.1}$$

with the assumed decomposition

$$\left|M_{AB\to CiX'}\right|^2 = \frac{\bar{\phi}_B^2}{\left(p_\beta^2 - m_\beta^2\right)^2} \left|M_{\beta A\to iX'}\right|^2 \tag{II.2}$$

and

$$dp = \frac{d^4C}{(2\pi)^3}\, \delta^{(+)}\left(C^2 - m_C^2\right) \frac{d^4i}{(2\pi)^3}\, \delta^{(+)}\left(i^2 - m_i^2\right) \quad . \tag{II.3}$$

Here, the function $\bar{\phi}_B$ is the covariant vertex function for the particle C on-shell and β off-shell. We have therefore

$$E_C \frac{d\sigma}{dC^3}(AB\to CiX') = \frac{\bar{\phi}_B^2\,(p_\beta)}{\left(p_\beta^2 - m_\beta^2\right)^2} \frac{1}{2E_A 2E_B \left|v_A - v_B\right|} \left|M_{\beta A\to iX'}\right|^2 \frac{d^3i}{E_i} \quad . \tag{II.4}$$

We assume that the off-shell continuation of the matrix element is smooth so that we can identify

$$\frac{1}{(1-x)2E_A 2E_B \left|v_A - v_B\right|} \left|M_{\beta A\to iX'}\right| = E_i \frac{d^3\sigma}{di^3}(\beta A\to iX') \quad , \tag{II.5}$$

where x is the fractional momentum of C out of B. The inclusive cross section for $AB \to CX$ is obtained from (II.4) by integrating over (d^3i/E_i):

$$E_C \frac{d^3\sigma}{dC^3}(AB\to CX) = (1-x) \frac{\bar{\phi}_B^2\,(p_\beta)}{\left(p_\beta^2 - m_\beta^2\right)^2} \sum_i \int \frac{d^3i}{E_i} E_i \frac{d^3\sigma}{di^3}(\beta A\to iX') \quad . \tag{II.6}$$

Noting that the baryon propagations of b and β (when they are off-shell) are related by

$$\frac{p_b^2 - m_b^2}{p_\beta^2 - m_\beta^2} = \frac{x}{1 - x} \quad , \tag{II.7}$$

we can rewrite the following factor in (II.6) as

$$(1 - x) \frac{\bar{\phi}_B^2 (p_\beta)}{\left(p_\beta^2 - m_\beta^2\right)^2} = x \frac{x}{1 - x} \frac{\bar{\phi}_B^2 (p_\beta)}{\left(p_b^2 - m_b^2\right)^2} \quad . \tag{II.8}$$

The result of (I.8) suggests the usefulness of introducing

$$\bar{G}_{C/B}\left(x, \vec{C}_T\right) = \frac{x}{1 - x} \frac{\bar{\phi}_B^2 (p_\beta)}{\left(p_b^2 - m_b^2\right)^2} \quad , \tag{II.9}$$

which differs with $G_{C/B}(x, \vec{C}_T)$ only in the vertex function: the vertex function is evaluated when the particle C is on-shell for $G_{C/B}(x, \vec{C}_T)$ and is evaluated when C is off-shell for $G_{C/B}(x, \vec{C}_T)$. In terms of $\bar{G}$, the invariant cross section for $AB \to CX$ is

$$E_C \frac{d^3\sigma}{dC^3} = x\bar{G}_{C/B}\left(x, C_T\right) \sum_i \int \frac{d^3 i}{E_i} E_i \frac{d^3\sigma}{di^3} (\beta A \to iX') \quad . \tag{II.10}$$

FIGURE CAPTIONS

Fig. 1. (a) Diagrams for the direct fragmentation process leading to $A + B \rightarrow C + X$.

(b) Diagrams for the hard-scattering process leading to $A + B \rightarrow C + X$.

Fig. 2. Experimental invariant cross section of Anderson et al.,[10] for the $\alpha + {}^{12}C \rightarrow p + X$ reaction plotted as a function of the scaling variable x_D. Different types of data points are used for different projectile momentum per nucleon, as indicated. Figure 2(a) is for a proton transverse momentum $p_T = 0$, 2(b) is for $p_T = 0.15$ GeV/c, and 2(c) is for $p_T = 0.3$ GeV/c.

Fig. 3. Comparison of experimental data of Anderson et al.,[10] with the theoretical results for the reaction $\alpha + {}^{12}C \rightarrow p + X$ at a projectile momentum of 1.74 GeV/c per nucleon. Figure 3(a) is for proton transverse momentum $p_T = 0$ and 3(b) is for $p_T = 0.3$ GeV/c. The solid curve is the theoretical cross section which is the sum of the direct fragmentation component represented by the dashed curve, and the hard-scattering component represented by the dashed-dot curve.

Fig. 4. Comparison of the transverse momentum distribution of Anderson et al.,[10] with the theoretical results for $\alpha + {}^{12}C \rightarrow p + X$ at a projectile momentum of 1.74 GeV/c per nucleon and the detected proton at a momentum of 1.75 GeV/c. The solid curve is the theoretical cross section which is the sum of the direct fragmentation cross section (the dashed curve) and the hard-scattering cross section (the dashed-dot curve).

Fig. 5. Comparison of experimental data of Anderson et al.,[10] with the theoretical results for $\alpha + {}^{12}C \rightarrow p + X$ at a projectile momentum of 2.88 GeV/c per nucleon. Figure 5(a) is for $p_T = 0$, and 5(b) is for $p_T = 0.3$ GeV/c. The solid curve is the theoretical cross section which is the sum of the direct fragmentation component (the dashed curve) and the hard scattering component (the dashed-dot curve).

Fig. 6. Same as in Fig. 4, but for a projectile momentum of 2.88 GeV/c/N.

Fig. 7. The semi-emperical momentum distribution of a nucleon in the ^4He nucleus as determined by the present analysis (solid curve) is compared with theoretical distributions (labeled curves) calculated by Zabolitzky and Ey.[13] The labeled curves are the theoretical momentum distributions obtained by using different interactions: SSCB for de Tourreil-Sprung super soft core potential, RSC for Reid soft core potential, and HJ for Hamada-Johnston potential. All are obtained by including nucleon correlations. The uncorrelated result is given by the curve labeled UNC.

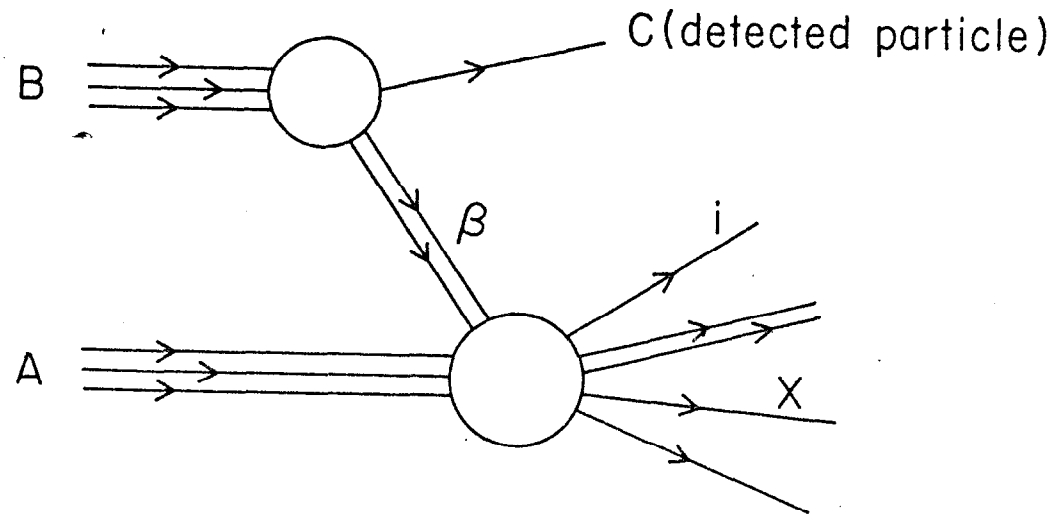

(a) Direct Fragmentation

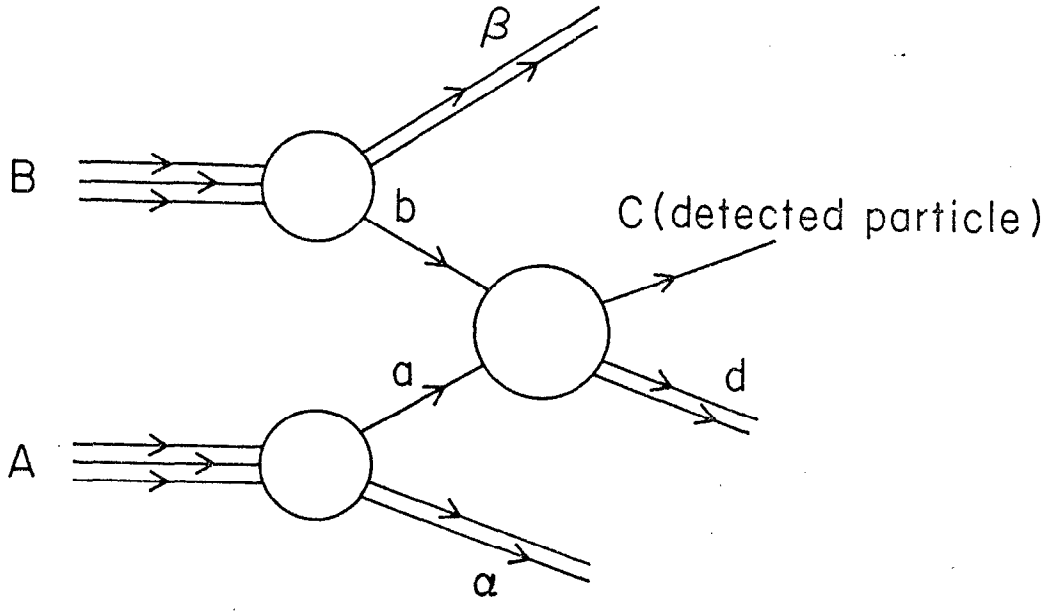

5-80

(b) Hard Scattering

3865A1

Fig. 1

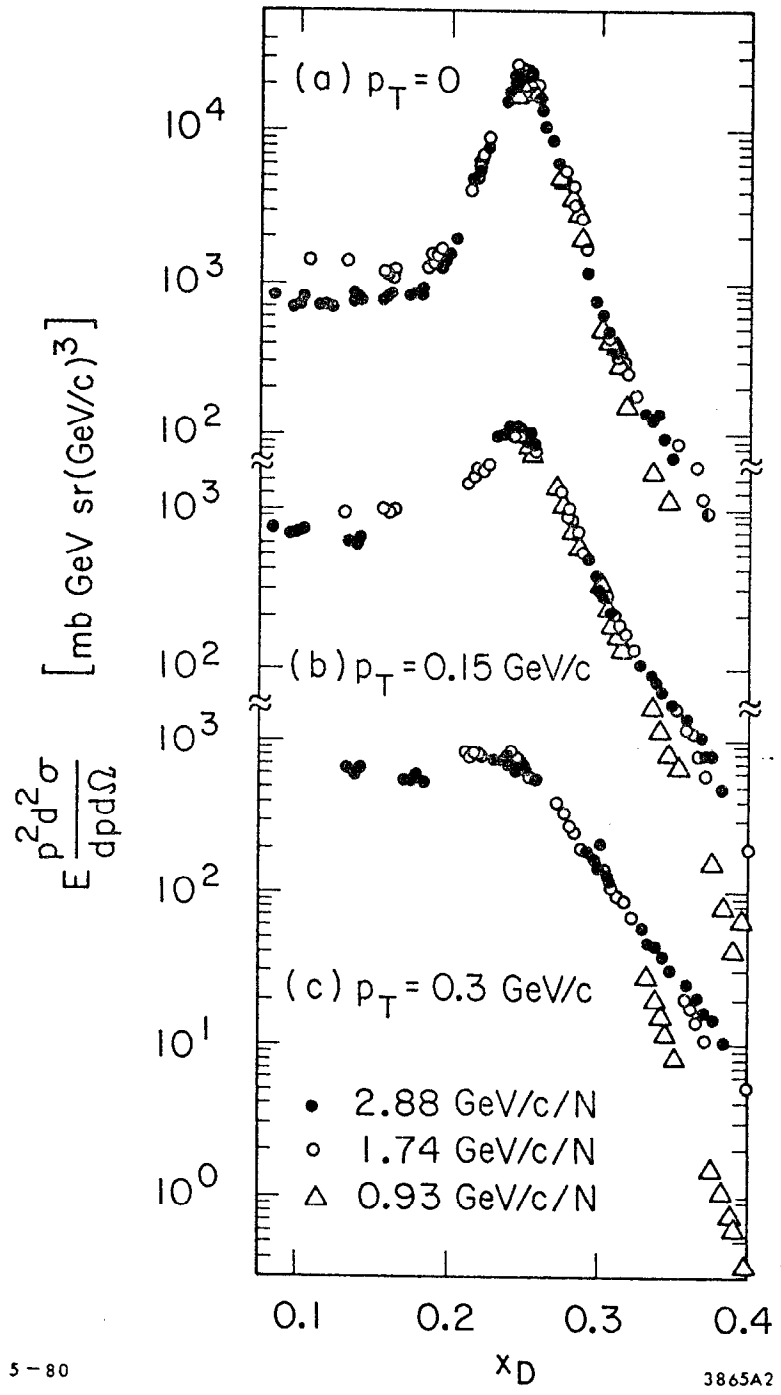
(a) $p_T = 0$
(b) $p_T = 0.15$ GeV/c
(c) $p_T = 0.3$ GeV/c
2.88 GeV/c/N
1.74 GeV/c/N
0.93 GeV/c/N
$E\frac{p^2d^2\sigma}{dpd\Omega}$ [mb GeV sr(GeV/c)^3]
10^4
10^3
10^2
10^3
10^2
10^3
10^2
10^1
10^0
0.1
0.2
0.3
0.4
x_D
5-80
3865A2

Fig. 2

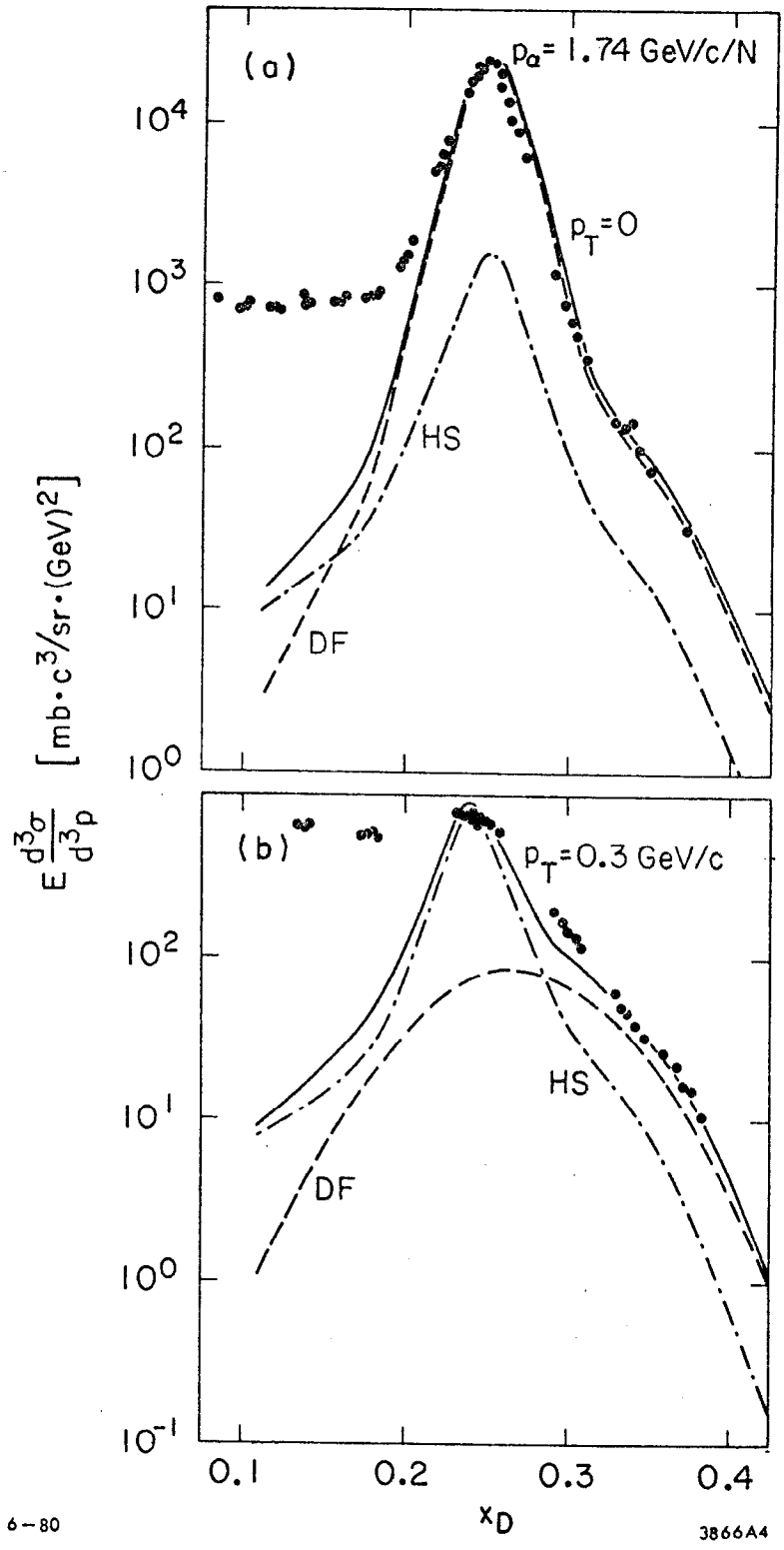
(a)
p_a= 1.74 GeV/c/N
p_T=0
HS
DF
(b)
p_T=0.3 GeV/c
HS
DF
$E\frac{d^3\sigma}{d^3p}$ [mb·c³/sr·(GeV)²]
10^4
10^3
10^2
10^1
10^0
10^{-1}
0.1
0.2
0.3
0.4
x_D
6-80
3866A4

Fig. 3

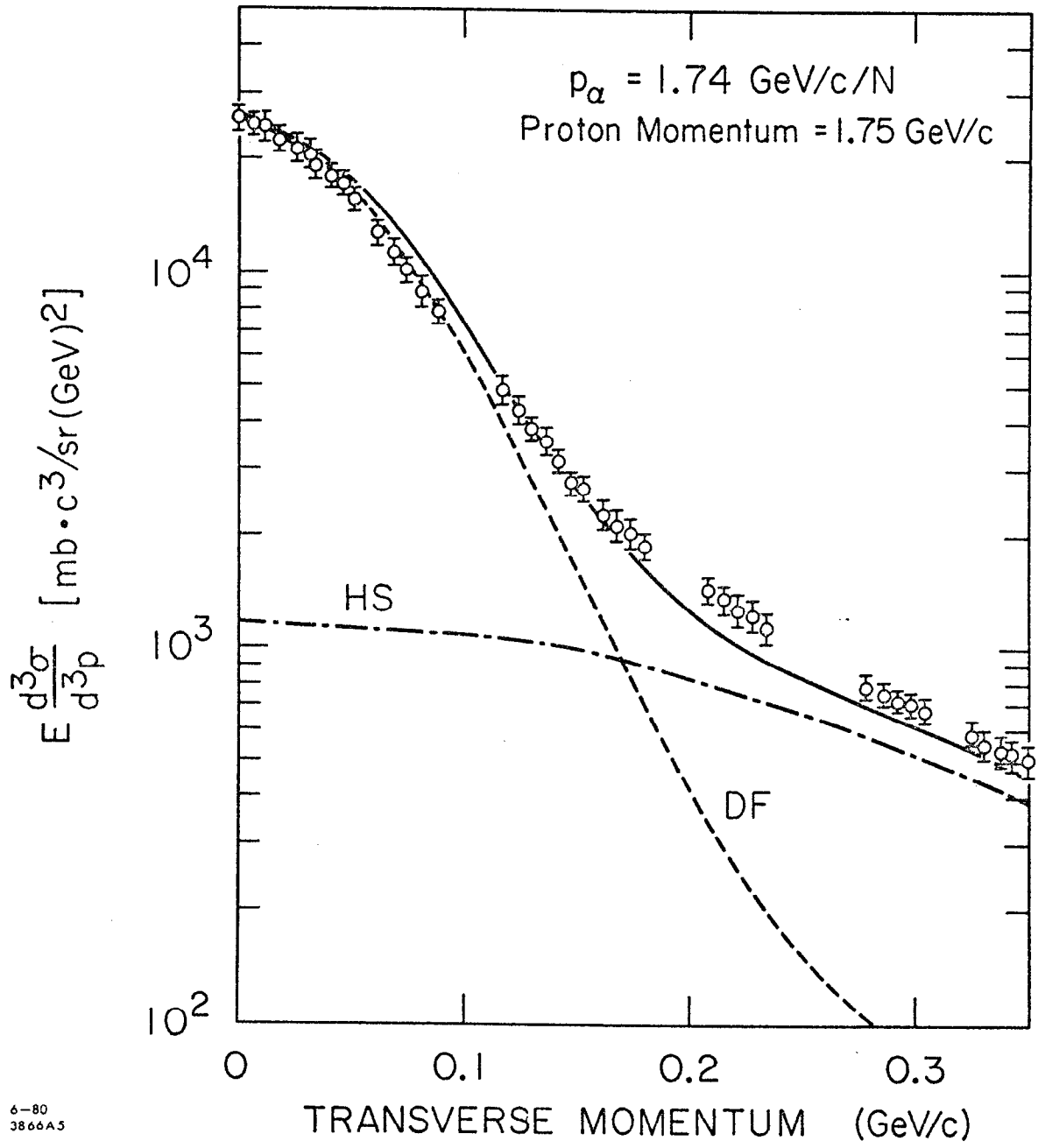
p_α = 1.74 GeV/c/N
Proton Momentum = 1.75 GeV/c
HS
DF
$E\frac{d^3\sigma}{d^3p}$ [mb • c^3/sr (GeV)^2]
10^4
10^3
10^2
0
0.1
0.2
0.3
TRANSVERSE MOMENTUM (GeV/c)
6-80
3866A5

Fig. 4

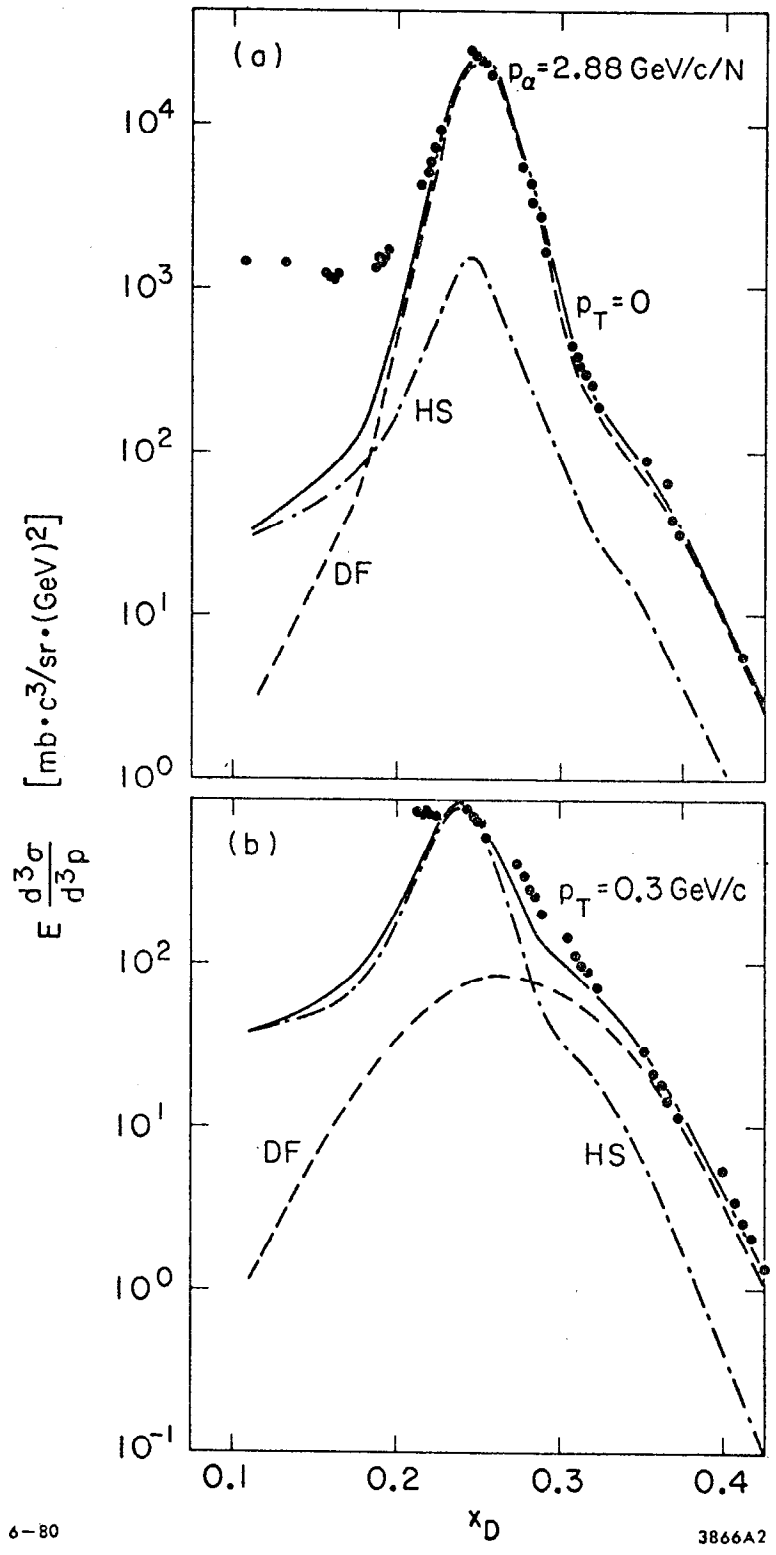
(a)
p_α=2.88 GeV/c/N
p_T=0
HS
DF
(b)
p_T=0.3 GeV/c
DF
HS
$E\frac{d^3\sigma}{d^3p}$ [mb•c³/sr•(GeV)²]
10^4
10^3
10^2
10^1
10^0
10^{-1}
0.1
0.2
0.3
0.4
x_D
6-80
3866A2

Fig. 5

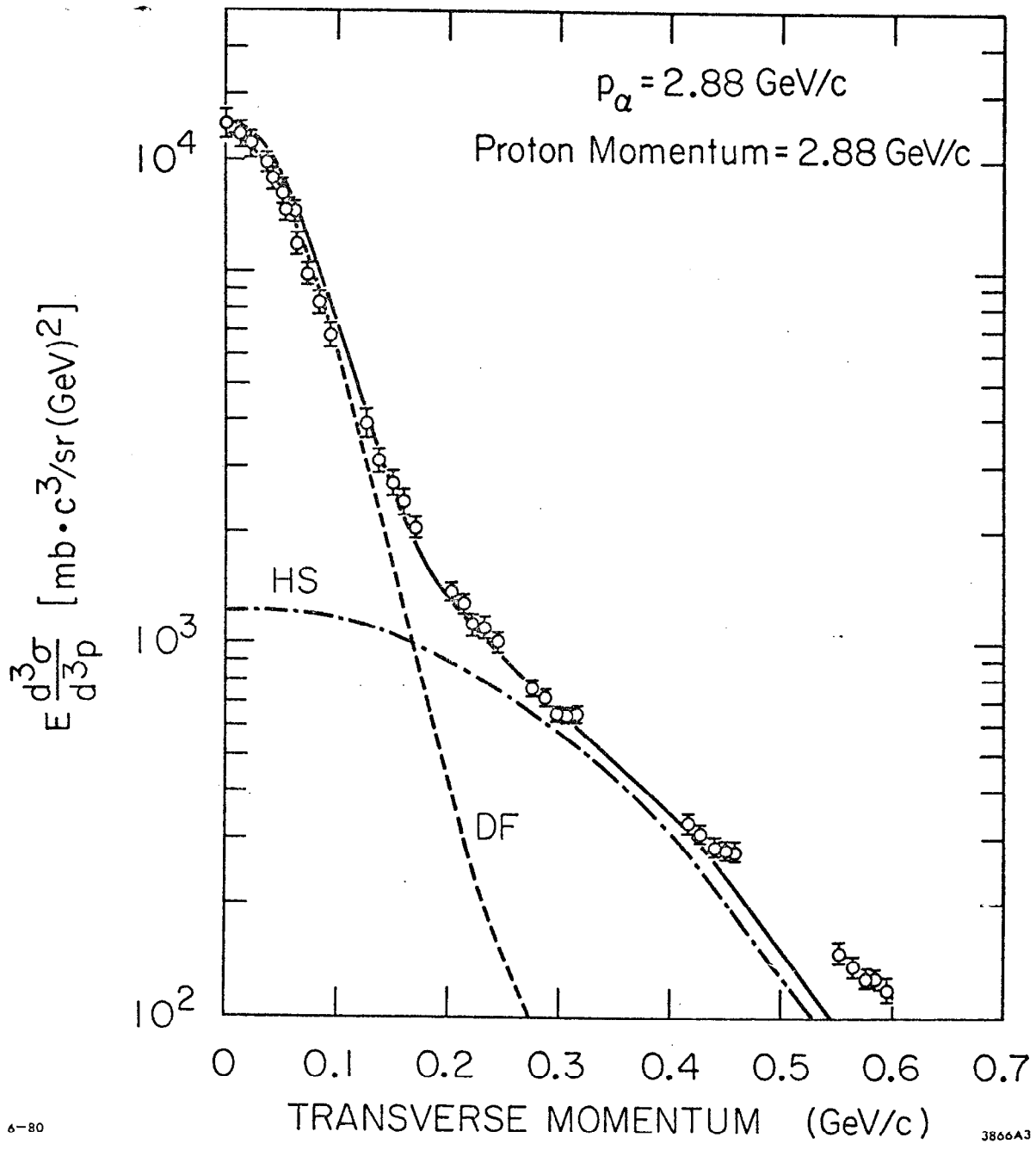
p_α = 2.88 GeV/c
Proton Momentum = 2.88 GeV/c
HS
DF
$E\frac{d^3\sigma}{d^3p}$ [mb • c³/sr (GeV)²]
10^4
10^3
10^2
0
0.1
0.2
0.3
0.4
0.5
0.6
0.7
TRANSVERSE MOMENTUM (GeV/c)
6-80
3866A3

Fig. 6

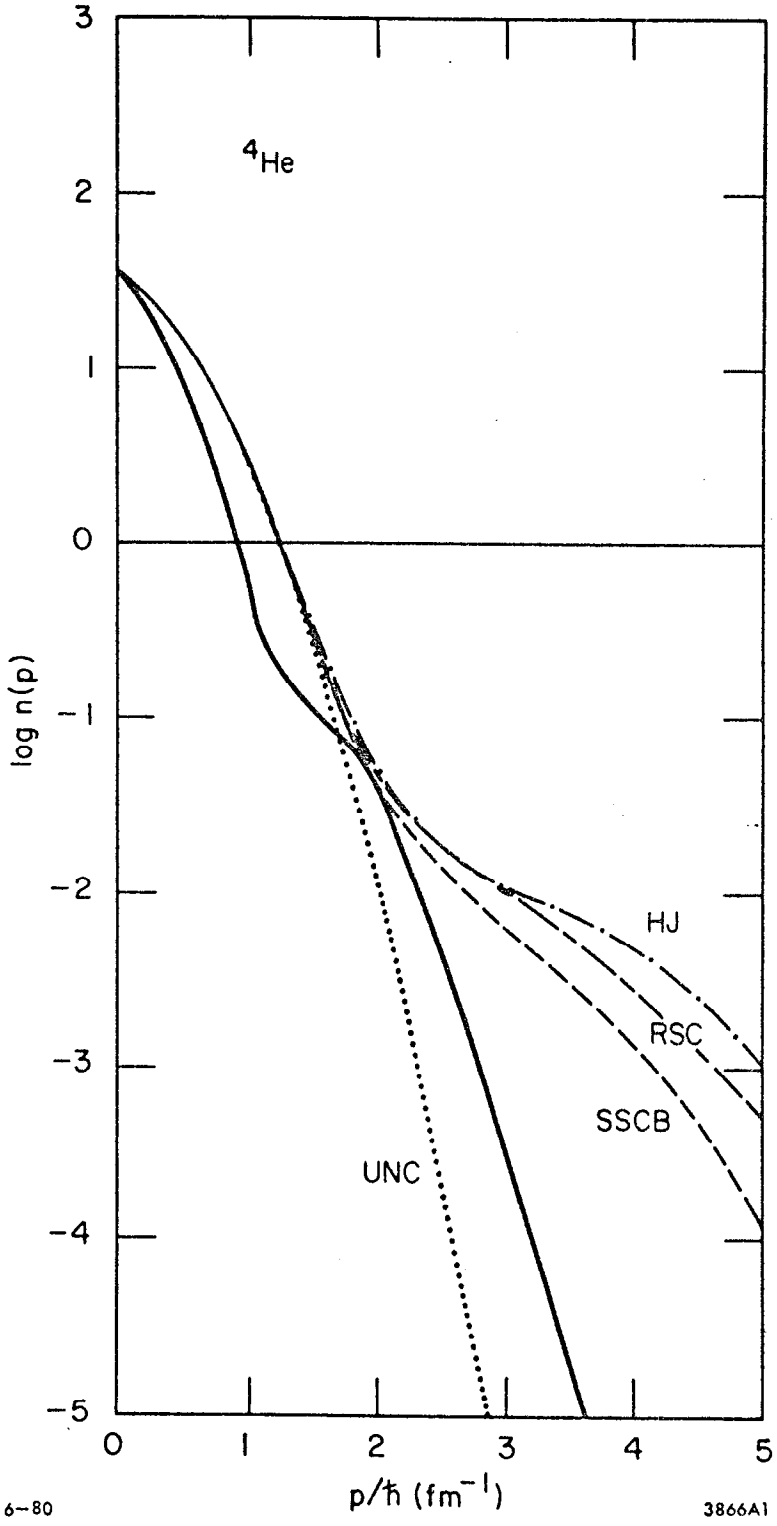

Fig. 7